Effect of Co2+ on oxygen reduction reaction catalyzed by Pt catalyst, and its implications for fuel cell contamination

Li, Hui; Tsay, Ken; Wang, Haijiang; Wu, Shaohong; Zhang, Jiujun; Jia, Nengyou; Wessel, Silvia; Abouatallah, Rami; Joos, Nathan; Schrooten, Jeremy

Publisher's version / Version de l'éditeur:
https://doi.org/10.1016/j.electacta.2009.12.037
Electrochimica Acta, 55 (2010), p. 2622–2628, 2009-12-29

Electrochimica Acta 55 (2010) 2622–2628

Contents lists available at ScienceDirect

Electrochimica Acta

journal homepage: www.elsevier.com/locate/electacta

Effect of Co^{2+} on oxygen reduction reaction catalyzed by Pt catalyst, and its implications for fuel cell contamination

Hui Li[a], Ken Tsay[a], Haijiang Wang[a], Shaohong Wu[a], Jiujun Zhang[a,*], Nengyou Jia[b], Silvia Wessel[b], Rami Abouatallah[c], Nathan Joos[c], Jeremy Schrooten[d]

[a] Institute for Fuel Cell Innovation, National Research Council Canada, Vancouver, B.C., V6T 1W5, Canada
[b] Ballard Power Systems Inc., Burnaby, B.C., V5J 5J8, Canada
[c] Hydrogenics Corp., Mississauga, O.N., L5R 1B8, Canada
[d] Angstrom Power Inc., North Vancouver, B.C., V7P 3N4, Canada

ARTICLE INFO

Article history:
Received 18 November 2009
Received in revised form
15 December 2009
Accepted 16 December 2009
Available online 29 December 2009

Keywords:
Oxygen reduction reaction
Cobalt ion contamination
Proton exchange membrane fuel cells
ORR kinetics
ORR mechanism

ABSTRACT

The oxygen reduction reaction (ORR) catalyzed by Pt was studied in the presence of Co^{2+} using cyclic voltammetry (CV), rotating disk electrode (RDE), and rotating ring-disk electrode (RRDE) techniques in an effort to understand fuel cell cathode contamination caused by Co^{2+}. Findings indicated that Co^{2+} could weakly adsorb on the Pt surface, resulting in a slight change in ORR exchange current densities. However, this weak adsorption had no significant effect on the nature of the ORR rate determining steps. The results from both RDE and RRDE indicated that the overall electron transfer number of the ORR in the presence of Co^{2+} was reduced, with ~9% more H_2O_2 being produced. We speculate that the weakly adsorbed Co^{2+} on Pt could react with the H_2O_2 intermediate and form a Co^{2+}–H_2O_2 intermediate, inhibiting the further reduction of H_2O_2 and thus resulting in more H_2O_2 production. The fuel cell performance drop observed in the presence of Co^{2+} could be attributed to the reduction in overall electron transfer number and the increase in H_2O_2 production. Higher production could intensify the attack by H_2O_2 and its radicals on membrane electrode assembly components, including the ionomer, carbon support, Pt particles, and membrane, leading to fuel cell degradation.

1. Introduction

Insufficient durability/reliability and high cost are two major challenges hindering the commercialization of proton exchange membrane (PEM) fuel cells. To address these issues, researchers have made tremendous efforts in recent years to develop new cost-effective materials, understand the mechanisms of performance degradation, and devise strategies for failure mode mitigation [1,2].

The major degradation modes of PEM fuel cells are connected to the low stabilities of the key materials, including Pt-based catalysts and proton exchange membranes, in a fuel cell operating environment. The major catalyst degradation modes are considered to be Pt agglomeration and dissolution, catalyst support (carbon) corrosion or oxidation, and catalyst contamination [3–5].

With regard to the catalyst contamination, impurities from feed streams (both air and fuel) and fuel cell components are the primary catalyst contaminants. In the last several years, significant progress has been made in identifying impurity sources and understanding their impacts on fuel cell performance [6–14]. For example, the primary impurities in hydrogen fuel are CO, H_2S, NH_3, and hydrocarbons deriving mainly from hydrogen-rich reformate gas; the major impurities in the air stream include NO_x (NO_2 and NO), SO_x (SO_3 and SO_2), and CO_x (CO_2 and CO), as well as some volatile organic compounds (VOCs). Other impurities involve metal ions, including Fe^{3+}, Cu^{2+}, Cr^{3+}, and Co^{2+}, from fuel cell components such as the catalysts/catalyst layers, gas diffusion layers, membrane, bipolar plates, sealing, and manifolds. All of these impurities have some contamination effects on the catalysts, leading to fuel cell degradation. For example, CO and H_2S, two ubiquitous fuel impurities, degrade performance mainly through strong preferential adsorption on the Pt surface, occupying active sites that would otherwise be used for the hydrogen oxidation reaction (HOR) [15,7]. NO_x and SO_x from air can also strongly adsorb on the Pt surface, blocking active sites for the oxygen reduction reaction (ORR) and reducing fuel cell performance [16,6].

In the literature, the major observation about metal ions' impact on fuel cell performance is their effect on membrane conductivity [17–21]. Unfortunately, how metal ions affect fuel cell catalysts has received very little attention. It was reported that a perfluorinated cation exchange membrane could easily absorb foreign metal ions, because the positive multi-charged metal ions had a stronger affinity for the negatively charged sulfonic acid group (SAG) than did

* Corresponding author. Tel.: +1 604 221 3087; fax: +1 604 221 3001.
E-mail address: jiujun.zhang@nrc.gc.ca (J. Zhang).

0013-4686/$ – see front matter.
doi:10.1016/j.electacta.2009.12.037

H^+ [22]. Different possible modes of fuel cell degradation through metal ion contamination have also been discussed [22]. In the first mode, metal ions get into the membrane and alter its bulk properties, e.g., by lowering membrane ionic conductivity, water content, and H^+ transference numbers. In the second mode, the presence of metal ions alters the water flux inside the membrane by changing the electroosmotic drag and the diffusion coefficient of water, and in the third mode, metal ions affect the ionomer in the cathode catalyst layer and lower the catalyst layer's proton conductivity.

While few studies have looked at how metal ions affect catalyst activity [18,19,23,24], we believe it is necessary to initiate such an investigation, particularly in the case of Pt alloys being used as the cathode ORR catalyst, where a second alloy metal such as Co could leach out during fuel cell operation. In the current state of PEM fuel cell technology, Pt alloys are a new generation of cathode ORR catalysts, mainly because they exhibit higher ORR activity/stability and contain less Pt than pure Pt catalysts. A $Pt_3Ni(111)$ skin catalyst reportedly yielded an activity 10 times higher than a Pt(111) catalyst, and 90 times higher than a Pt/C catalyst [25], a $PtAuNi_5/C$ catalyst achieved 3.3 times more mass activity than Pt/C in a PEM single cell test [26], and a PtCoMn alloy catalyst exhibited a durability of over 7300 h, exceeding the DOE 2010 target of 5000 h [27]. In addition, because of their low cost, non-platinum catalysts based on non-noble metals such as Fe [28] and Co [29] are considered sustainable cathode ORR catalysts. However, a major drawback of these low-Pt and non-Pt catalysts is metal dissolution [30–32]. For example, for Pt–Co alloys or Co-based non-Pt catalysts, Co dissolution becomes a major issue in a PEM fuel cell operating environment. The dissolution of Co^{2+} may cause fuel cell contamination, leading to performance degradation. Similar to other metal ions [33–35], Co^{2+} may exchange with H^+ in both the membrane and the ionomer of the catalyst layer, and/or adsorb on the Pt catalyst surface, and/or change the hydrophobicity of the catalyst layer and/or gas diffusion layer (GDL), resulting in low fuel cell performance.

We therefore believe it is important to study the effect of Co^{2+} on fuel cell Pt catalysts. In our laboratory, fuel cell contamination testing and diagnosis in the presence of Co^{2+} were conducted under various conditions, and performance degradation was clearly observed even with trace amounts of cobalt ion. In order to fundamentally understand the effect of Co^{2+} contamination on fuel cell performance, in this paper we report our electrochemical studies of the effect of Co^{2+} on the kinetics and mechanisms of the ORR catalyzed by Pt catalyst. Cyclic voltammetry (CV), rotating disk electrode (RDE), and rotating ring-disk electrode (RRDE) techniques were employed to examine to what degree Co^{2+} could affect the kinetics and mechanisms of the ORR in sulfuric acid solution. We hope this study will provide important insights into PEM fuel cells in which Co^{2+} is inevitably present due to the leaching effect of Pt alloy and non-Pt catalysts, even though the quantitative effect may be somewhat different during PEM fuel cell operation due to differences in Co^{2+} concentration, water activity, ionic environment, and operating conditions.

2. Experimental

2.1. Working electrode and electrolyte solution preparation

For the RDE measurements, a bare Pt disk electrode with a geometric area of 0.20 cm^2 (Pine Instruments) was used as the rotating disk electrode (the working electrode). For the RRDE set-up, a glassy carbon (GC) disk electrode with a geometric area of 0.25 cm^2 (Pine Instruments) was used as the disk electrode on which a thin catalyst layer was coated to form a working electrode. Prior to the catalyst layer coating, the glassy carbon disk electrode was polished to a mirror finish with 0.05 μm alumina (Buehler). For catalyst layer preparation, a commercially available carbon-supported Pt powder (Pt/C, 46.9 wt% Pt, purchased from TKK) was used to make the catalyst ink. The ink was prepared by ultrasonically dispersing the as-received Pt/C catalyst powder for 30 min in a solution consisting of ethanol (Sigma–Aldrich), DI water (18 MΩ cm, Millipore Milli-Q system) and 5% Nafion® ionomer (Alfa-Aesar). The weight ratio of Nafion® to Pt/C in this catalyst ink was 1:21. The ink was then pipetted onto the glassy carbon disk surface with a Pt loading of 40 $\mu g\,cm^{-2}$, forming a catalyst layer. After air-drying, this working electrode was transferred into the electrochemical cell for measurements.

The base electrolyte solution used in this paper was 0.5 M H_2SO_4, prepared using reagent-grade sulfuric acid (Acros). For surface cyclic voltammograms, this base solution was deaerated by purging with nitrogen (99.999%, Praxair) for 30 min before each measurement. For catalyst ORR activity measurements, this base solution was saturated with oxygen (99.999%, Praxair) through constant bubbling for 10 min before each measurement, and was kept bubbling during the measurements. For Co^{2+} contamination measurements, the electrolyte containing Co^{2+} was made by dissolving cobalt sulfate hydrate (Sigma–Aldrich) into the 0.5 M H_2SO_4 solution.

2.2. Electrochemical measurements

Electrochemical measurements were conducted in a standard three-electrode electrochemical cell using an RDE or RRDE as the working electrode. For RRDE experiments, two Solartron 1287 potentiostats were used to control the disk and ring potentials, respectively, and an AFMRX rotator (Pine Instruments) controlled the rotating speed. For both RDE and RRDE measurements, a platinum-black-coated Pt wire and a mercury sulfate electrode were used as counter and reference electrodes, respectively. In the RRDE set-up, a Pt ring was used to detect the formation of H_2O_2, and the collection coefficiency of this Pt ring was calibrated as 0.37. The electrochemical cell temperature was controlled by a water bath. During electrochemical measurements, the freshly prepared working electrode was immersed in the electrolyte and electrochemically cleaned by repeatedly cycling the potential between 0.03 and 1.3 V vs. RHE for more than 20 cycles at a scan rate of 100 $mV\,s^{-1}$. Surface CV was then performed with potential sweeping between 0.05 and 1.2 V vs. RHE at 50 $mV\,s^{-1}$ in a deaerated 0.5 M H_2SO_4 solution with or without Co^{2+} present, and the electrode surface was determined to be clean when a reproducible voltammogram of expected form was recorded. The ORR measurements were performed by linear sweep voltammetry between 0.05 and 1.0 V vs. RHE at 5 $mV\,s^{-1}$ in O_2-saturated 0.5 M H_2SO_4 solution with or without Co^{2+} present. For RRDE measurements, the potential of the Pt ring electrode was kept at 1.2 V vs. RHE, where the oxidation of hydrogen peroxide was under pure diffusion control.

2.3. Fuel cell contamination testing in the presence of Co^{2+}

The membrane electrode assembly (MEA) consisted of an Ion Power catalyst-coated membrane (CCM) and SGL gas diffusion layers. The MEA had an active area of 50 cm^2, with 0.4 $mg\,cm^{-2}$ Pt loadings on both anode and cathode sides. To introduce the contaminant Co^{2+}, a 2.8×10^{-3} M of $CoSO_4$ salt solution was injected into the air feeding stream in the fuel cell cathode side at a constant flow rate of 0.2 $mL\,min^{-1}$, which provided a contaminant level of 5 ppm mol Co^{2+}/mol air. The contamination tests were carried out in a constant-current discharge mode, during which cell voltage was recorded as a function of time. For comparison, a baseline test was carried out under the same fuel cell operating condi-

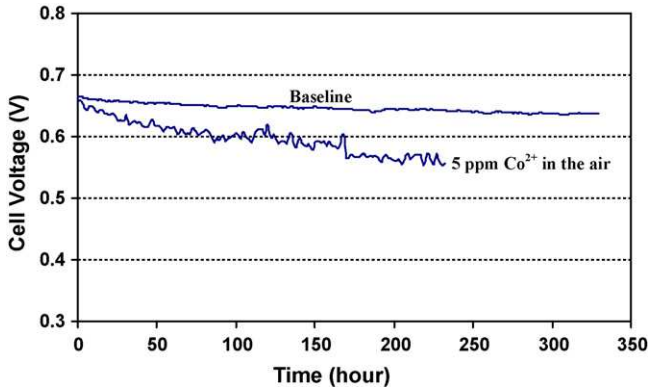

Fig. 1. Cell voltage vs. time during contamination testing with 5 ppm Co^{2+} in the air stream (mol Co^{2+}/mol air). Conditions: RH = 100%; cell temperature = 80 °C; backpressure = 15 psig; stoichiometries = 1.5 for H_2 and 3.0 for air; current density = 1.0 A cm^{-2}. Pt loading: 0.4 μg cm^{-2} on both anode and cathode sides.

tions as the contamination test but without the injection of any liquid.

3. Results and discussion

3.1. Fuel cell cathode contamination in the presence of Co^{2+}

Fig. 1 shows fuel cell voltage as a function of testing time in the absence and presence of Co^{2+}, measured at a current density of 1.0 A cm^{-2}, cell temperature of 80 °C, backpressure of 15 psig, and stoichiometries of 1.5/3.0 for H_2/air.

In the presence of Co^{2+}, an obvious performance drop appears, and increases with testing time until the cell voltage reaches a plateau. This observation clearly indicates that Co^{2+} has a negative effect on the cathode reaction, resulting in fuel cell degradation. In our laboratory, Co^{2+} contamination tests were conducted at different temperatures and Co^{2+} concentrations. In order to understand the contamination effect of Co^{2+}, various diagnostic measurements, such as electrochemical impedance spectra (EIS), cathode surface CVs, and hydrogen crossover, were also performed at different stages during the contamination process. Detailed results and discussions will be reported in a follow-on publication. In brief, our EIS measurements identified three contributors to the performance drop caused by Co^{2+}: slower ORR kinetics (electron transfer rate), increased membrane resistance, and slower mass transfer. In this paper, we will only focus on the effect of Co^{2+} on ORR kinetics and the implications for fuel cell cathode contamination. To this end, ex-situ electrochemical measurements in a conventional three-electrode cell, including CV, RDE, and RRDE, were carried out under different conditions in the presence of Co^{2+}. Based on these results, we propose mechanisms for Co^{2+} contamination effects on ORR kinetics and mechanisms.

3.2. Cyclic voltammograms recorded on Pt catalyst in the three-electrode cell

To investigate the effect of Co^{2+} on cathode Pt catalyst, surface CVs were recorded in a 0.5 M H_2SO_4 electrolyte solution containing 0.05 M Co^{2+}, within a three-electrode cell. For comparison, the same CV was also recorded in the absence of Co^{2+}. Typical CVs for both cases are shown in Fig. 2, from which two observations can be drawn. First, compared to the curve without Co^{2+}, the curve in the presence of Co^{2+} contains no cobalt redox peaks other than those of platinum oxide on the Pt surface during the cathodic and anodic scans, indicating that Co^{2+} had no electrochemical activity in the potential range 0.05–1.2 V vs. RHE. Second,

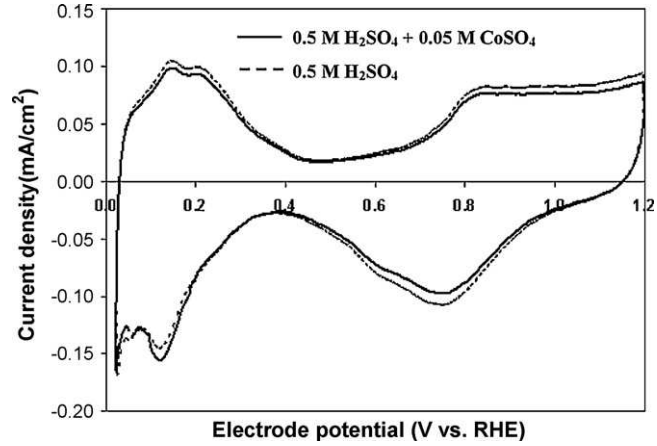

Fig. 2. Cyclic voltammograms for bare Pt electrode at 25 °C in 0.5 M H_2SO_4 (dashed) and 0.5 M H_2SO_4 + 0.05 M $CoSO_4$ (solid), respectively. Electrode potential scan rate: 50 mV s^{-1}.

the areas beneath the hydrogen adsorption–desorption peaks were not significantly reduced after Co^{2+} was added to the electrolyte solution, suggesting that the adsorption of Co^{2+} on the Pt surface was weaker than that of hydrogen atoms. From the areas under the hydrogen adsorption–desorption peaks, the electrochemical Pt surface areas (EPSAs) of the catalyst can be calculated using the well-recognized Coulombic charge of hydrogen adsorption on a Pt surface, 210 C cm^{-2}. The obtained EPSA values in the presence and absence of 0.05 M Co^{2+} are 46 and 49 m^2 g^{-1} Pt, respectively, which equate to a reduction of ~6% in the EPSA. Although it might be arguable that this reduction of ~6% falls close to the error associated with the EPSA measurement, the trend of reduced EPSA in the presence of Co^{2+} was observed in many similar tests. Therefore, this reduction probably represents the effect of Co^{2+} (or Co^{2+} weak adsorption) on the active reaction area of the Pt catalyst.

3.3. RDE results in the presence of Co^{2+}

3.3.1. Polarization curves

In order to understand the effect that weak adsorption of Co^{2+} has on the ORR kinetics and mechanism, RDE measurements were performed in a 0.5 M H_2SO_4 electrolyte containing various levels of Co^{2+}.

Using a bare Pt disk electrode, polarization curves were obtained at 25 °C by linearly scanning the electrode potential from 1.0 to 0.2 V vs. RHE at a sweep rate of 5 mV s^{-1}. Fig. 3 shows the polarization curves collected at two rotation rates with various levels

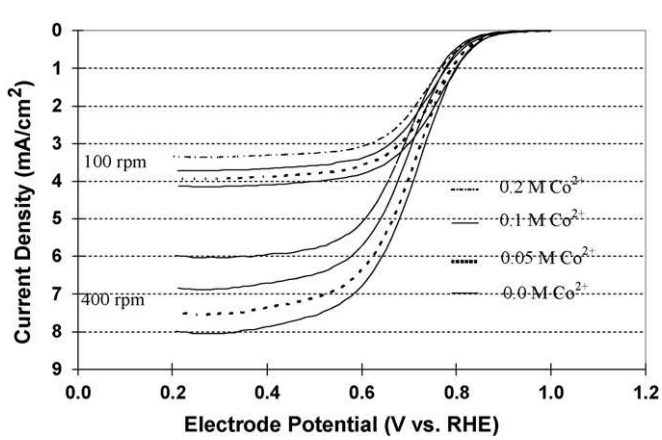

Fig. 3. Polarization curves for the ORR on a bare Pt RDE, at 25 °C in 0.5 M H_2SO_4 solutions containing various levels of Co^{2+}. Potential scan rate: 5 mV s^{-1}.

of $CoSO_4$ in O_2-saturated 0.5 M H_2SO_4 electrolyte solution. A well-defined plateau can be obtained for each curve after the electrode potential is below 0.5 V, indicating a diffusion-controlled process in the potential range 0.2–0.5 V. However, in the potential range 1.0–0.5 V, the curves should represent a mixed process of kinetics and diffusion. Compared to the polarization curves obtained in the absence of Co^{2+}, those in the presence of various Co^{2+} levels exhibited lower current densities at all potentials, indicating that both kinetic and diffusion rates of the ORR were reduced. In addition, as the concentration of Co^{2+} rose, the reduction in current densities became more significant, suggesting that weak adsorption of Co^{2+} on the Pt surface is a function of the concentration of Co^{2+} in the electrolyte.

3.3.2. Overall electron transfer number

The reduction of kinetic currents in the presence of Co^{2+} (Fig. 3) may be attributed to two factors: (1) decrease in the ORR electron transfer rate, and (2) change in the ORR mechanisms (the fraction of the 4-electron transfer pathway to H_2O for the overall mechanism decreases, and at the same time, the fraction of the 2-electron transfer pathway to H_2O_2 increases). The increase in the latter pathway to H_2O_2 might also promote a reduction in the diffusion currents. For example, the plateau current in Fig. 3 can be expressed in a Levich form:

$$\frac{I_d}{A} = i_d = 0.62nFC_{O_2}D_{O_2}^{2/3}\nu^{-1/6}\omega^{1/2} \quad (1)$$

where I_d is the disk plateau current (diffusion-limiting current), i_d the disk plateau current density (diffusion-limiting current density), A the electrode diffusion area, n the overall number of transferred electrons in the ORR process, F the Faradaic constant, C_{O_2} the oxygen concentration, D_{O_2} the oxygen diffusion coefficient, ν the kinematic viscosity of the electrolyte, and ω the electrode rotation rate. From Eq. (1) it can be seen that the reduced plateau currents in the presence of Co^{2+}, as observed in Fig. 3, may have been caused by changes in n, A, C_{O_2}, D_{O_2}, and ν. To simplify the matter, we assume that the changes in the values of A, C_{O_2}, D_{O_2}, and ν are insignificant compared to the change in the value of n, caused by the presence of Co^{2+}. In other words, reductions in diffusion-limiting currents such as the plateau currents in Fig. 3 may derive mainly from a reduction in the overall electron transfer number of the ORR.

To quantitatively estimate the change in the electron transfer number, the Koutecky–Levich equation is employed to correlate the disk current density (i) with the diffusion-limiting current density (i_d):

$$\frac{1}{i} = \frac{1}{i_k} + \frac{1}{i_d} \quad (2)$$

where i_k is the kinetic current density for the ORR and i_d the diffusion-limiting current density, as expressed in Eq. (1). It should be noted that the disk current densities (i) were all mass-transport corrected according to Eq. (3):

$$E = E^o + \frac{2.303RT}{\alpha n_\alpha F}\log(i^o) - \frac{2.303RT}{\alpha n_\alpha F}\log\left(\frac{i_d i}{i_d - i}\right) \quad (3)$$

where E is the electrode potential, E^o the electrode potential for the ORR under standard conditions (E^o = 1.23 V vs. RHE), R the universal gas constant, T the temperature, n_α and α are, respectively, the electron transfer number and electron transfer coefficient in the rate determining step of the ORR, F the Faradaic constant, and i^o the exchange current density of the catalyzed ORR.

Fig. 4 shows the Koutecky–Levich plots (i^{-1} vs. $\omega^{-1/2}$) for the ORR with and without Co^{2+} in the electrolyte solution, together with theoretical plots for the 2-electron and 4-electron transfer processes of the ORR. In the absence of Co^{2+}, the plot is essentially parallel to the theoretical 4-electron plot, indicating that the ORR catalyzed by Pt/C is a process close to the 4-electron transfer process that produces water; the electron transfer number was calculated from the slope to be 3.95. However, when Co^{2+} was added to the 0.5 M H_2SO_4 electrolyte, the Koutecky–Levich plots moved away from the theoretical plot for the 4-electron transfer process, indicating that Co^{2+} in the solution shifted the ORR mechanism more towards the 2-electron transfer process, producing H_2O_2. Taking the slopes of the plots, the overall electron numbers at different levels of Co^{2+} were calculated using Eq. (1) and are given in Table 1. Clearly, as the concentration of Co^{2+} increased, the overall electron transfer number decreased from 3.95 at 0.0 M Co^{2+} to 3.42 at 0.2 M Co^{2+}. The change in the overall electron transfer number in the presence of Co^{2+} represents the effect of Co^{2+} on the ORR mechanism.

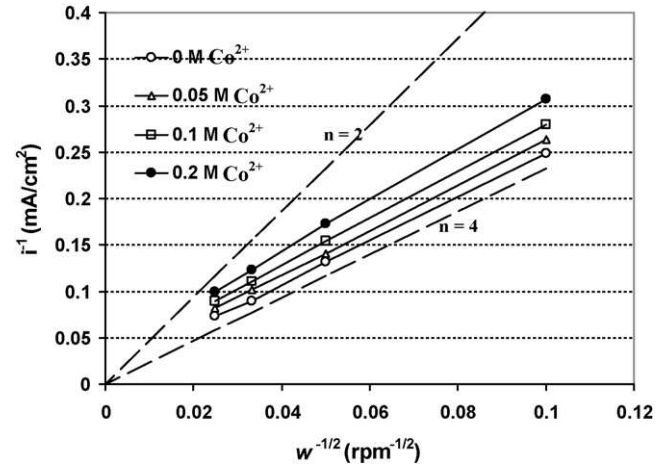

Fig. 4. Koutecky–Levich plots for the ORR on bare Pt RDE, at 25 °C in 0.5 M H_2SO_4 solutions containing various levels of Co^{2+}. Potential scan rate: 5 mV s^{-1}.

3.4. RRDE results in the presence of Co^{2+}

In addition to conducting RDE measurements using the bare Pt disk electrode as the working electrode, we also carried out RRDE measurements using the Pt/C catalyst-coated GC disk electrode as the working electrode to further study the effect of Co^{2+} on the ORR. Fig. 5 shows the ring and disk currents obtained at two rotation rates, at 25 °C with 0.05 M $CoSO_4$ present in the 0.5 M H_2SO_4 electrolyte. The potential of the ring electrode was set at 1.2 V, where the oxidation of the H_2O_2 formed by the ORR on the disk electrode was diffusion-limited.

3.4.1. Tafel plots

Using the disk currents shown in Fig. 5, Tafel plots in the absence and presence of 0.05 M Co^{2+} were obtained (Fig. 6) to help understand whether or not the ORR electron transfer rate was reduced by the presence of Co^{2+}. The current densities in the Tafel plots were also mass-transport corrected according to Eq. (3).

In Fig. 6, each Tafel plot has two different slopes, corresponding to the high electrode potential region (>~0.8 V vs. RHE) and low electrode potential region (<~0.8 V), respectively. From the CV curves shown in Fig. 2, it can be seen that at a potential of ~0.8 V

Table 1
Overall electron transfer numbers for ORR on bare Pt RDE at 25 °C in 0.5 M H_2SO_4 solutions containing various levels of Co^{2+} (calculated from the Koutecky–Levich plots shown in Fig. 4).

Concentration of Co^{2+} in the electrolyte (M)	0.0	0.05	0.1	0.2
Overall electron transfer numbers	3.95	3.84	3.68	3.42

Table 2
Tafel slopes and exchange current densities (i_0) for the ORR on Pt/C catalyst.

Electrolyte	Tafel slopes (mV dec^{-1})		log(i_0) (A cm^{-2})	
	High electrode potential	Low electrode potential	High electrode potential	Low electrode potential
0.5 M H_2SO_4	−77	−132	−8.0	−5.7
0.5 M H_2SO_4 + 0.05 M $CoSO_4$	−78	−132	−7.6	−5.5

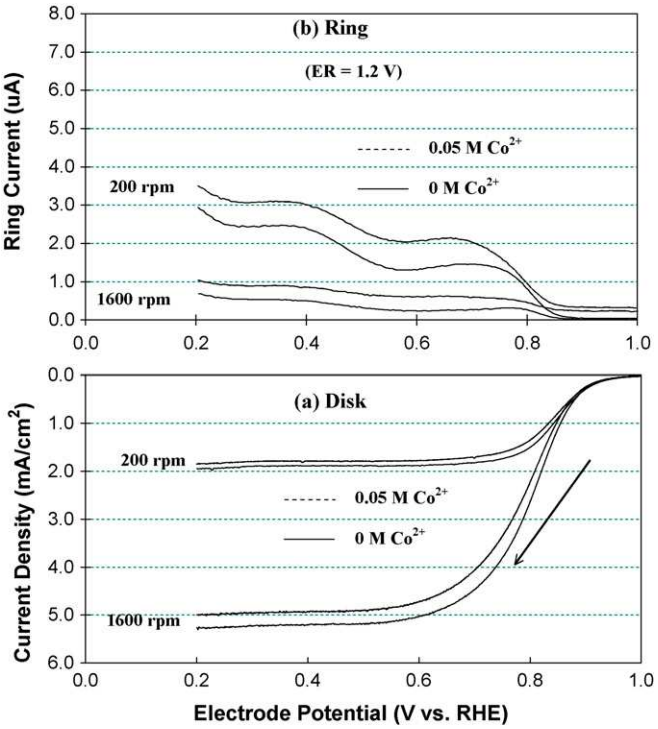

Fig. 5. (a) Disk current densities at 200 and 1600 rpm for the ORR on an RRDE coated with Pt/C catalyst (Pt loading: 40 μg cm^{-2}) at 25 °C in 0.5 M H_2SO_4 solutions saturated with 1 atm O_2. Potential scan rate: 5 mV s^{-1}. (b) Ring currents at 200 and 1600 rpm with a ring potential of E_R = 1.2 V vs. RHE. Dashed curves: with 0.05 M Co^{2+} in the electrolyte. Solid curves: without 0.05 M Co^{2+} in the electrolyte.

vs. RHE, the Pt surface should contain a mixed surface structure of PtO/Pt, which has been reported in the literature [36]. This redox couple ($PtO + 2e^- + 2H^+ \leftrightarrow Pt + H_2O$) has an electrode potential of 0.88 V vs. RHE under standard conditions, which is very close to the potential at the joining point of the two lines of a Tafel plot

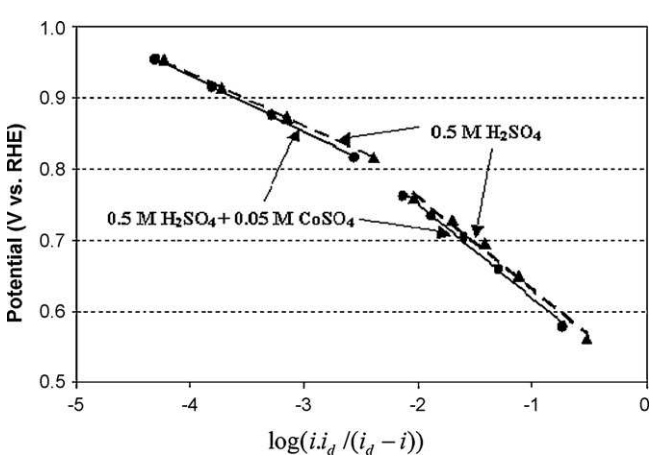

Fig. 6. Tafel plots of the ORR on an RDE coated with a thin catalyst layer (Pt loading: 40 μg cm^{-2}), obtained from negative sweeps at 1600 rpm in 0.5 M H_2SO_4 and 0.5 M H_2SO_4 + 0.05 M $CoSO_4$, respectively, at 25 °C. Data from Fig. 5.

in Fig. 6. This means that when the electrode potential is higher than 0.8 V the dominant surface species is PtO, while the dominant species becomes pure Pt when the electrode potential is less than 0.8 V. Therefore, we believe that the Tafel line at a high electrode potential should represent the ORR process on a PtO surface, and the Tafel line at a low potential should correspond to the ORR process on a pure Pt surface [36]. In the absence of Co^{2+}, the two Tafel slopes at the high and low electrode potentials were determined to be 77 and 132 mV dec^{-1}, respectively, from the Tafel plot shown in Fig. 6. Based on the Tafel slope expression shown in Eq. (3) (i.e., $2.303RT/\alpha n_\alpha F$) and assuming that the electron transfer number (n_α) for the ORR in the rate determining step is 1, the electron transfer coefficient (α) was calculated to be 0.77 and 0.45 for the high and low electrode potential regions, respectively. When 0.05 M Co^{2+} was added to the test solution, a two-part Tafel plot was obtained, as shown in Fig. 6. It can be seen that the effect on the Tafel slopes of having 0.05 M Co^{2+} in the electrolyte was insignificant considering the uncertainty associated with fitting the Tafel slope, suggesting that the presence of 0.05 M Co^{2+} could not change the nature of the rate determining step in the ORR process in both high and low potential regions. However, Co^{2+} in the electrolyte did result in a slight downward shift of the two Tafel lines in both regions, equivalent to logarithmic decreases in the exchange current densities from −7.6 to −8.0 and −5.5 to −5.7, respectively, as listed in Table 2. These small gaps between the plots for the presence and absence of 0.05 M Co^{2+} indicate that both rates in the ORR rate determining step can be slightly reduced with the addition of Co^{2+} ions. Normally, the exchange current density represents the intrinsic reaction rate of the rate determining step of the ORR (i.e., the first electron transfer step), and therefore the slight decrease in the exchange current density caused by the presence of Co^{2+} suggests that the ions slightly lowered the reaction rate of the ORR rate determining step. As discussed earlier with Fig. 2, the EPSA was reduced in the presence of Co^{2+} due to the weak adsorption of Co^{2+} on the Pt surface. Therefore, we believe that the decrease in exchange current density in the presence of Co^{2+} should also be closely related to this weak adsorption. In other words, the weak adsorption of Co^{2+} ion on the Pt surface may have reduced the ORR intrinsic exchange current density, resulting in a lower ORR rate.

3.4.2. H_2O_2 production yield

Fig. 5 shows that the presence of Co^{2+} apparently could increase the ring currents, indicating that more H_2O_2 was produced. To quantify the formation of H_2O_2 in the absence and presence of Co^{2+}, hydrogen peroxide yields (%H_2O_2) at different rotating rates were calculated at a disk electrode potential of 0.5 V vs. RHE, using Eq. (4):

$$\%H_2O_2 = \frac{(I_r/I_d)}{N} \times 100 \quad (4)$$

where I_r and I_d are the currents at the ring and disk electrodes, respectively, and N the RRDE collection coefficient of 0.37 as provided by the electrode supplier and confirmed by our experiments.

As Fig. 7 shows, at a disk potential of 0.5 V vs. RHE, the presence of 0.05 M Co^{2+} in the electrolyte solution increased the hydrogen peroxide yield by ~9% at different rotation rates. This result clearly indicates that the portion of the 4-electron transfer pathway pro-

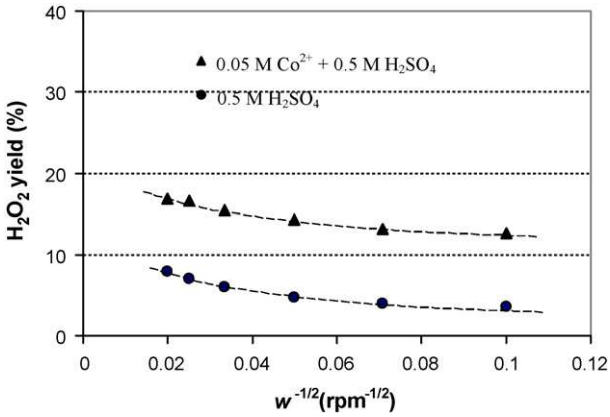

Fig. 7. Percentage of H_2O_2 formation in the absence and presence of 0.05 M Co^{2+}, respectively, in 0.5 M H_2SO_4 electrolyte saturated with 1 atm O_2 on an RRDE coated with Pt/C catalyst (Pt loading: 40 μg cm^{-2}) at 25 °C. Calculated at 0.5 V vs. RHE from the data in Fig. 5.

ducing H_2O decreased and at the same time, the portion of the 2-electron transfer pathway producing H_2O_2 increased.

3.5. Exploration of Co^{2+} contamination mechanism

As is generally recognized, the ORR catalyzed by a Pt catalyst follows a complex reaction mechanism during which oxygen adsorbed on the Pt surface can be electrochemically reduced through a series of elementary steps. In general, adsorbed H_2O_2 is produced after two electrons are transferred. However, this H_2O_2 can then either be further reduced to water or dissolve into the solution. Depending on the type, surface structure, and purity of the catalyst, the ratio of H_2O_2 being further reduced to water to the amount of H_2O_2 dissolving into the solution varies. Apparently, the ORR mechanism on a pure Pt surface is not necessarily the same as on a PtO surface. As discussed earlier, when the electrode potential is lower than 0.8 V vs. RHE, the dominant species on the Pt catalyst surface is pure Pt. Therefore, here we limit our attention to a pure Pt surface.

Based on the literature [37–40], the ORR mechanism on a Pt catalyst is proposed to follow a series of steps, as given in Reactions (I)–(V):

$$\text{Pt} + \text{O}_2 \rightarrow \text{Pt-O}_{2(\text{ads})} \quad \text{(I)}$$

$$\text{Pt-O}_{2(\text{ads})} + \text{H}^+ + \text{e}^- \rightarrow \text{Pt-O}_2\text{H}_{(\text{ads})} \quad (\text{ratedeterminingstep}) \quad \text{(II)}$$

$$\text{Pt-O}_{2(\text{ads})} + \text{e}^- + \text{H}^+ \rightarrow \text{Pt-O}_2\text{H}_{2(\text{ads})} \quad \text{(III)}$$

$$x(\text{Pt-O}_2\text{H}_{2(\text{ads})}) + 2x\text{H}^+ + 2x\text{e}^- \rightarrow x\text{Pt} + 2x(\text{H}_2\text{O}) \quad \text{(IV)}$$

$$(1-x)(\text{Pt-O}_2\text{H}_{2(\text{ads})}) \rightarrow (1-x)\text{Pt} + (1-x)\text{H}_2\text{O}_2 \quad \text{(V)}$$

In this mechanism, Reaction (II) represents the ORR rate determining step on a Pt surface, i.e., the first electron transfer step, and Reaction (III) represents the formation of adsorbed H_2O_2 on the Pt surface. There are then two pathways for the adsorbed H_2O_2 to follow: further reduction to H_2O through Reaction (IV), or chemical desorption through Reaction (V) to form free H_2O_2 that enters the bulk solution. When an RRDE is used, the free H_2O_2 is spun away from the disk electrode and detected by the ring electrode. The former pathway will form a 4-electron transfer mechanism for the ORR to produce H_2O, and the latter will form a 2-electron transfer mechanism to produce H_2O_2. In reality, the ORR normally has a mixed 2- and 4-electron transfer pathway, giving an overall electron transfer number of less than 4. The relative proportions of 2- and 4-electron transfer pathways are dependent on Reactions (IV) and (V). The portion of Reaction (IV) can be expressed as x and that of Reaction (V) as $(1-x)$. If $x = 1$, the mechanism will be an entirely 4-electron transfer pathway, and if $x = 0$, the mechanism will become a totally 2-electron pathway. In normal situations, x is between 0 and 1, giving a mixed 2- and 4-electron transfer pathway. When Co^{2+} is present in the electrolyte, the value of x becomes smaller than when Co^{2+} is absent. In other words, the relative proportion of the H_2O_2 production expressed by Reaction (V) in the presence of Co^{2+} becomes larger when compared to the production in the absence of Co^{2+}. The effect of weakly adsorbed Co^{2+} on the ORR mechanism may occur mainly through Co^{2+} reacting with the intermediate $\text{Pt-O}_2\text{H}_{2(\text{ads})}$ produced by Reaction (III):

$$\text{Pt-O}_2\text{H}_{2(\text{ads})} + \text{Co}^{2+} \rightarrow \text{Pt} + [\text{Co-H}_2\text{O}_2]^{2+}_{\text{sol}} \quad \text{(VI)}$$

The complex $[\text{Co-H}_2\text{O}_2]^{2+}_{\text{sol}}$ may be more stable than $\text{Pt-O}_2\text{H}_{2(\text{ads})}$, inhibiting the further reduction of $\text{Pt-O}_2\text{H}_{2(\text{ads})}$ through Reaction (IV), and thus leading to an increase in the proportion of Reaction (V), i.e., an increase in the value of $1-x$. As a result, more H_2O_2 would be produced in the presence of Co^{2+}. However, this is simply speculation, and more experiments are needed to confirm this hypothesis.

3.6. Implications for fuel cell contamination

As discussed above, the ORR reaction mechanism can be affected by the presence of Co^{2+}. The major effect is a reduction in the overall electron transfer number of the ORR, resulting in more H_2O_2 production. This could partially contribute to the fuel cell degradation observable in Fig. 1.

First, the reduction in overall electron transfer number after the injection of Co^{2+} into the cathode compartment will lead to a decrease in fuel cell current density. During constant-current contamination testing, fuel cell voltage must drop in order to maintain a constant current density. Second, H_2O_2 and its radicals are commonly known to attack the ionomer, carbon support, and Pt particles inside the catalyst layer, as well as the proton exchange membrane. Therefore, the increased H_2O_2 production in the presence of Co^{2+} intensifies the adverse effects of H_2O_2. Hydrogen peroxide attack has been recognized as a major factor in catalyst layer degradation modes (such as changes in catalyst layer hydrophilicity, carbon corrosion, and Pt particle isolation and dissolution), as well as in membrane degradation (conductivity reduction). More detailed fuel cell diagnostic results using EIS and other techniques to identify the degradation modes of Co^{2+} contamination will be presented in a follow-on publication.

Despite the importance of the information obtained through the RRDE technique in understanding the contamination mechanisms of Co^{2+} on the cathode catalyst, it has to be realized that there are differences between the conditions in the RRDE tests and fuel cell tests, such as differences in Co^{2+} concentration, water activity, ionic environment, and operating conditions. Therefore, the quantitative effect of Co^{2+} contamination during PEM fuel cell operation may be somewhat different than in RRDE tests.

4. Conclusions

Cobalt is a potential element for Pt alloy catalysts in PEM fuel cells, but it is known that cobalt can leach out from the alloy catalysts and hence becoming a contaminant, causing degradation in fuel cell performance. Therefore, electrochemical study of the adverse effects of Co^{2+} on the ORR has practical implications for fuel cell contamination caused by the presence of Co^{2+}.

In this paper, the ORR on both bare Pt and Pt/C catalysts was studied in the presence of Co^{2+} using CV, RDE, and RRDE tech-

niques. Cyclic voltammograms obtained in the presence of 0.05 M Co^{2+} revealed that Co^{2+} could weakly adsorb on the Pt surface. However, this weakly adsorbed Co^{2+} could not change the rate determining step of the ORR, and could only slightly decrease the exchange current densities. The results from RDE measurements indicate that the overall electron transfer number of the ORR was reduced from 3.95 in the absence of Co^{2+} to 3.84, 3.68, and 3.42 when 0.05, 0.1, and 0.2 M Co^{2+}, respectively, were present in the 0.5 M H_2SO_4 electrolyte. RRDE results with Pt/C catalysts suggested that the H_2O_2 production yield increased by about 9% when 0.05 M Co^{2+} was present in the electrolyte.

With respect to the change in ORR mechanisms caused by the presence of Co^{2+}, we speculate that Co^{2+} weakly adsorbed on the Pt catalyst could react with Pt-$O_2H_{2(ads)}$, an adsorbed H_2O_2 intermediate, to form $[Co\text{-}H_2O_2]^{2+}_{sol}$, impeding the further reduction of H_2O_2 to water and thus resulting in greater H_2O_2 concentration.

In terms of the fuel cell performance drop during contamination testing with Co^{2+} in the cathode side, the reduction in overall electron transfer number caused by Co^{2+} weakly adsorbed on the Pt catalyst could contribute to decreased fuel cell voltage during operation in a constant-current mode. In addition, more H_2O_2 production in the presence of Co^{2+} could result in a more intensive attack by H_2O_2 and its radicals on the components (ionomer, carbon support, Pt catalyst particles, and membrane) inside the membrane electrode assembly, leading to fuel cell degradation.

References

[1] J. Wu, X.Z. Yuan, J. Martin, H. Wang, J.J. Zhang, J. Shen, S. Wu, W. Merida, J. Power Sources 184 (2008) 104.
[2] S. Zhang, X.Z. Yuan, J.C. Hin, H. Wang, K.A. Friedrich, M. Schulze, J. Power Sources 194 (2009) 588.
[3] X. Cheng, Z. Shi, N. Glass, L. Zhang, J. Zhang, D. Song, Z.S. Liu, H. Wang, J. Shen, J. Power Sources 165 (2007) 739.
[4] H. Li, Z. Shi, J.J. Zhang, in: J. Garche (Ed.), Encyclopedia of Electrochemical Power Sources, Elsevier, Oxford, UK, 2009 (chapter 874).
[5] H. Li, C. Song, J.L. Zhang, in: J.J. Zhang (Ed.), PEM Fuel Cell Electrocatalysts and Catalyst Layers: Fundamentals and Applications, Springer, Springer-Verlag London Ltd., Surrey, UK, 2008 (chapter 6).
[6] D. Yang, J. Ma, L. Xu, M. Wu, H. Wang, Electrochim. Acta 51 (2006) 4039.
[7] W. Shi, B. Yi, M. Hou, F. Jing, H. Yu, P. Ming, J. Power Sources 164 (2007) 272.
[8] H. Li, J.L. Zhang, Z. Shi, D. Song, K. Fatih, S. Wu, H. Wang, J.J. Zhang, N. Jia, S. Wessel, R. Abouatallah, N. Joos, J. Electrochem. Soc. 156 (2009) B252.
[9] Z. Shi, D. Song, H. Li, K. Fatih, Y. Tang, J.L. Zhang, Z. Wang, S. Wu, Z. Liu, H. Wang, J.J. Zang, J. Power Sources 186 (2009) 435.
[10] H. Li, J.L. Zhang, Z. Shi, D. Song, K. Fatih, S. Wu, J.J. Zhang, N. Jia, S. Wessel, R. Abouatallah, N. Joos, ECS Trans. 16 (2008) 1059.
[11] H. Li, J.L. Zhang, K. Fatih, Z. Wang, Y. Tang, Z. Shi, S. Wu, D. Song, J.J. Zhang, N. Jia, S. Wessel, R. Abouatallah, N. Joos, J. Power Sources 185 (2008) 272.
[12] J.J. Zhang, H. Wang, D. Wilkinson, D. Song, J. Shen, Z.S. Liu, J. Power Sources 147 (2005) 58.
[13] Z. Shi, D. Song, J.J. Zhang, Z.S. Liu, S. Knights, R. Vohra, N. Jia, D. Harvey, J. Electrochem. Soc. 154 (2007) B609.
[14] R. Halseid, P.J.S. Vie, R. Tunold, J. Power Sources 154 (2006) 343.
[15] H.F. Oetjen, V.M. Schmidt, U. Stimming, F. Trila, J. Electrochem. Soc. 143 (1996) 3838.
[16] F. Jing, M. Hou, W. Shi, J. Fu, H. Yu, P. Ming, B. Yi, J. Power Sources 166 (2007) 172.
[17] T. Okada, N. Nakamura, J. Electrochem. Soc. 144 (1997) 2744.
[18] T. Okada, J. Electroanal. Chem. 465 (1999) 1.
[19] T. Okada, J. Electroanal. Chem. 465 (1999) 18.
[20] A. Collier, H. Wang, X.Z. Yuan, J. Zhang, D. Wilkinson, Int. J. Hydrogen Energy 31 (2006) 1838.
[21] M. Kelly, B. Egger, G. Fafilek, J.O. Besenhard, H. Kronberger, G.E. Nauer, Solid State Ionics 176 (2005) 2111.
[22] T. Okada, in: W. Vielstich, H.A. Gasteiger, A. Lamm (Eds.), Handbook of Fuel Cells—Fundamentals, Technology and Applications, vol. 3, John Wiley & Sons Ltd., Chichester, UK, 2003 (chapter 468).
[23] A. Pozio, R.F. Silva, M.D. Francesco, L. Giorgi, Electrochim. Acta 48 (2003) 1543.
[24] T. Okada, S.M. Holst, O. Gorseth, S. Kjelstrup, J. Electroanal. Chem. 442 (1998) 137.
[25] V.R. Stamenkovic, B. Fowler, B.S. Mun, G. Wang, P.N. Ross, C.A. Lucas, N.M. Markovic, Science 315 (2007) 493.
[26] J. Zhang, K. Sasaki, E. Sutter, R.R. Adzic, Science 315 (2007) 220.
[27] M.K. Debe, R. Atanasoski, Annual Progress Report. 861, DOE Hydrogen Program, 2008.
[28] M. Lefevre, E. Proietti, F. Jaouen, J. Dodelet, Science 324 (2009) 71.
[29] P. Zelenay, E. Brosha, J. Chlistunoff, S. Conradson, F. Garzon, C. Johnston, R. Mukundan, J. Spendelow, J. Valerio, M. Wilson, Annual Progress Report. 838, DOE Hydrogen Program, 2007.
[30] H.A. Gasteiger, S.S. Kocha, B. Sompalli, F.T. Wagner, Appl. Catal. B: Environ. 56 (2005) 9.
[31] N. Wakabayashi, M. Takeichi, H. Uchida, M. Watanabe, J. Phys. Chem. B 109 (2005) 5836.
[32] H.R. Colon-Mercado, H. Kim, B.N. Popov, Electrochem. Commun. 6 (2004) 795.
[33] M. Shi, F.C. Anson, J. Electroanal. Chem. 425 (1997) 117.
[34] M. Ohashi, C.S. Smith, J.W. Van Zee, ECS Trans. 11 (2007) 877.
[35] T. Okada, J. Phys. Chem. B 103 (1999) 3315.
[36] C. Song, Y. Tang, J.L. Zhang, J.J. Zhang, H. Wang, J. Shen, S. McDermid, J. Li, P. Kozak, Electrochim. Acta 52 (2007) 2552.
[37] B. Wang, J. Power Sources 152 (2005) 1.
[38] K. Kinoshita, Electrochemical Oxygen Technology, Wiley, New York, 1992.
[39] E. Yeager, Electrochim. Acta 29 (1984) 1527.
[40] E. Yeager, J. Mol. Catal. 38 (1986) 5.